ACCSCIENCE PUBLISHING

Journal of Energy and Sustainability

ORIGINAL RESEARCH ARTICLE

Kinetic analysis and process optimization of carbon dioxide hydrogenation to methanol over copper/zinc oxide/self-pillared pentasil-zeolite catalyst

Xiaolong Liu[1], Guangying Fu[1], Ruiqin Ding[1], Ke Liang[2], Qiaolin Lang[1]*, and Xiaobo Yang[3]*

[1]Key Laboratory of Photoelectrochemical Conversions, Qingdao Institute of Bioenergy and Bioprocess Technology, Chinese Academy of Sciences, Qingdao, Shandong, China

[2]Tianjin Passion Advanced Material Technology LLC., Binhai, Tianjin, China

[3]R&D Division, Vitalite ApS, Allerød, Hovedstaden, Denmark

Abstract

Hydrogenation of carbon dioxide (CO_2) using hydrogen generated by renewable electricity-powered water electrolysis is a key technology for producing e-fuels and supporting other carbon capture, utilization, and storage applications. Studies on reaction kinetics, reactors, and process engineering have predominantly focused on copper (Cu)/zinc oxide (ZnO)/aluminum oxide catalysts. This study analyzes the reaction kinetics of CO_2 hydrogenation into methanol and carbon oxide using a novel catalyst composed of Cu, ZnO, and self-pillared pentasil (SPP) zeolite. The one-site microkinetic model developed by Vanden Bussche and Froment was applied to fit initial laboratory-scale test data. The Cu/ZnO/SPP-zeolite catalyst demonstrates rapid kinetics and low apparent activation energy for methanol synthesis and the reversed water–gas shift reaction. As a result, it achieved an enhanced space-time yield of methanol at 1.75 $kg \cdot kg_{cat}^{-1}/h$ at 230°C and 50 bar in a single path simulation with a $CO_2/3H_2$ feed stream. Furthermore, a corresponding process optimization aiming at maximizing methanol yield was conducted, incorporating one recycling loop of the vapor products. The process simulation successfully converged with a 90% recycling rate, enabling the conversion of 2,000 NT of CO_2 per year, resulting in 1,836 NT of crude methanol at a concentration of 62.5 wt%. These findings provide a valuable addition to the existing literature.

Keywords: Carbon dioxide fixation; Carbon dioxide hydrogenation; Copper/zinc oxide/self-pillared pentasil-zeolite catalyst; Reaction kinetics; Process optimization

***Corresponding authors:**
Xiaobo Yang
(yangxiaobo@tjpassion.com)
Qiaolin Lang
(langql@qibebt.ac.cn)

Citation: Liu X, Fu G, Ding R, Liang K, Lang Q, Yang X. Kinetic analysis and process optimization of carbon dioxide hydrogenation to methanol over copper/zinc oxide/self-pillared pentasil-zeolite catalyst. *Journal of Energy and Sustainability*. 2025;1(2):025310015.
doi: 10.36922/JES025310015

Received: July 31, 2025

Revised: September 12, 2025

Accepted: September 12, 2025

Published online: October 7, 2025

1. Introduction

Hydrogenation of carbon dioxide (CO_2) using hydrogen sourced from renewable electricity-powered water electrolysis is recognized as a critical technology for producing e-fuels[1] and for various carbon capture, utilization, and storage applications. This method effectively utilizes captured CO_2 and stores intermittent renewable energy in liquid form.[2] Both traditional thermocatalytic processes and innovative

electrochemical catalytic methods for CO_2 reduction are currently being intensively investigated.[3,4] Among these strategies, converting CO_2 to methanol using catalysts with copper (Cu)/zinc oxide (ZnO)/aluminum oxide (Al_2O_3) compositions has emerged as a viable reaction technology.[5,6] An industrial demonstration project utilizing this technology has been in operation in Iceland since 2002 at a scale exceeding 2,000 NT/annum. The project has demonstrated a significant reduction in the carbon footprint per unit of energy production at the George Olah Plant.[7] However, the long-term operation has also indicated that CO_2 hydrogenation to methanol is not economically competitive with the conventional syngas-to-methanol process. The challenges arise from two main issues: The thermodynamic limitation surrounding the CO_2 conversion rate and the propensity for side reactions leading to carbon monoxide (CO) formation. In addition, the reactions produce water (H_2O) as a by-product, which can impede methanol formation by blocking active sites, causing structural changes, and even accelerating sintering of the active Cu metal particles when water accumulates in the catalyst.[8-10] Therefore, current research is directed toward improving Cu-based methanol catalysts and processes,[11] and developing novel catalysts[12-17] to enhance methanol space-time yields and extend catalyst lifetimes.

A promising strategy to enhance the performance of $Cu/ZnO/Al_2O_3$ catalysts involves replacing the alumina support with zeolites. Zeolites are crystalline materials characterized by uniform micropores, typically not larger than 1 nm, which can effectively confine small metal clusters. With appropriate modifications, the porous structure of zeolites can be engineered into a hierarchical system containing both micro- and mesopores, capable of accommodating larger metal particles. Using zeolites as catalyst supports offers significant advantages, including the uniform distribution of metal particles and protection against sintering through pore confinement.[18-21] Ultra-fine Cu particles of 1–2 nm stabilized within the grain boundaries of the nano-sized silicalite-1 zeolite have demonstrated high selectivity for methanol in CO_2 hydrogenation.[22] In addition, 2–8 nm Cu/ZnO composites have been successfully entrapped within the mesopores of self-pillared pentasil (SPP) zeolite, exhibiting greater activity than their $Cu/ZnO/Al_2O_3$ counterparts.[23] These findings align with the observations of other researchers, confirming that minimizing Cu particle size to a certain extent[24-27] and using zeolite supports[28-31] can improve CO_2 conversion and control product selectivity.

From a chemical engineering perspective, most investigations into reaction thermodynamics,[32,33] kinetics,[34-42] and reactor and process engineering,[43,44] have predominantly focused on $Cu/ZnO/Al_2O_3$ catalysts. Corresponding data regarding the catalytic reactions using other Cu-based catalysts, and those of different compositions, are relatively underrepresented in the literature.[45,46] This study analyzes the reaction kinetics of CO_2 hydrogenation to methanol and CO over a Cu/ZnO/SPP-zeolite catalyst, while optimizing processes to maximize methanol yield. The objective is to provide valuable data that may enhance the existing body of literature.

2. Materials and methods

2.1. Catalyst

Reagents used for catalyst preparation included tetraethoxysilane (>98%; Aladdin Scientific, United States), tetra-n-butylammonium hydroxide (25% in methanol; Aladdin Scientific, United States), copper(II) nitrate·$3H_2O$ (>99%; Macklin, China), zinc nitrate·$6H_2O$ (>99%; Sinopharm, China), and deionized water.

The pure-silica SPP zeolite was synthesized following a procedure adapted from Zhang *et al.*[47] The loading of Cu and Zn was achieved by impregnating the pure-silica SPP-zeolite with an aqueous solution of copper(II) nitrate, zinc nitrate, and ethylenediamine. Previous reports provide detailed descriptions of the preparation procedure and characterization of the catalyst.[23] Key characteristics of the material and the catalyst indicate that the pure-silica SPP-zeolite featured ellipsoidal particles approximately 100 nm in length, formed from intersecting nanoplates that are about 2 nm thick, enclosing voids with edge lengths ranging from 2 to 8 nm. The pure-silica version of the material was specifically selected to prevent further conversions of the product methanol into dimethyl ether, olefines, aromatics, and other products through acid-catalyzed reactions. The loading amounts of metal species were 25.6 wt% CuO and 11.2 wt% ZnO (calculated on the oxides). Calcined at 500°C in air, CuO nanoparticles of 2–8 nm diameter were observed to be evenly distributed across the zeolite using transmission electron microscopy. At the same time, ZnO was not detectable as an observable particle. Before catalytic tests, the material was reduced in a flow of 4 vol% H_2/argon at 400°C.

2.2. Catalytic test

The catalytic tests were conducted using a fixed-bed plug-flow microreactor (in-house built), with Φ = 0.4 mm and L = 50 mm (V_{bed} = 0.6 mL with 0.1 g catalyst deluded in quartz, grain sizes 150–250 μm). The feed consisted of a mixture of CO_2 and H_2 in volume ratios of 1:2, 1:3, or 1:4 at 30 mL/min (Standard Temperature and Pressure), and gas hourly space velocity = 3,000 h^{-1}. The activity was

assessed at 180–300°C under 30 or 50 bar pressures for 3 h at each temperature, increasing in 20°C intervals. The gas composition at the reactor outlet was analyzed using an online gas chromatograph (Agilent 7890A, US) equipped with an HP-Plot/Q column and a thermal conductivity detector. CO_2 conversion (X_{CO2}), methanol yield (Y_{CH3OH}), selectivity (S_{CH3OH}), and the space-time yield of methanol (STY_{CH3OH}) were calculated on a carbon basis using Equations I-IV, where N represents the fraction of each component in the reaction gas flow and M denotes the molar mass in g·mol^{-1}. The space-time yield, expressed in g·h^{-1}/g$_{cat}$, was calculated using $d_{cat/bed}$ = 0.1 g/0.6 mL.

$$X_{CO_2} = \frac{N_{CH_3OH} + N_{CO}}{N_{CO_2} + N_{CH_3OH} + N_{CO}} \times 100\% \quad \text{(I)}$$

$$Y_{CH_3OH} = \frac{N_{CH_3OH}}{N_{CO_2} + N_{CH_3OH} + N_{CO}} \times 100\% \quad \text{(II)}$$

$$S_{CH_3OH} = \frac{N_{CH_3OH}}{N_{CH_3OH} + N_{CO}} \times 100\% \quad \text{(III)}$$

$$STY_{CH_3OH} = GHSV \times \frac{0.25}{1000 \times 22.4} \times Y_{CH_3OH} \times \frac{M_{CH_3OH}}{d_{cat/bed}} \quad \text{(IV)}$$

2.3. Kinetic modeling

The apparent reaction rates were fitted to the Arrhenius equation, ln k = A + B/RT, where $r = k * \prod N^i$, with i representing the stoichiometric factor of each respective reagent in the reaction equation. The same apparent r values were utilized to fit the kinetics and thermodynamics parameters of the one-site kinetics model developed by Vanden Bussche and Froment (VBF).[41] The fitting results were then used in the simulations of both the reactor and the overall process.

3. Results and discussion

3.1. Catalytic tests in the microreactor

Catalytic tests were conducted in the temperature range of 200–300°C at pressures of 30 and 50 bar using a feed of CO_2 and H_2 at volume ratios of 1:2, 1:3, and 1:4, with a gas hourly space velocity of 3,000 h^{-1} in a diluted catalyst bed. Under the tested conditions, methanol (CH_3OH) and CO were the primary carbon-containing products, with trace amounts of methane, dimethyl ether, and ethanol detected as by-products. Consequently, two independent reactions were studied: (i) the CO_2 to methanol synthesis and (ii) the reversed water-gas shift (RWGS) reaction. The third reaction, the syngas-to-methanol reaction, can be seen as a combination of these two processes. The pure-silica version of SPP-zeolite prevented further acid-catalyzed conversions, such as methanol-to-dimethyl ether, the formation of olefin or aromatics, and oligomerizations and cracking. The reactions and the corresponding thermodynamic parameters are summarized in Table 1.[5,48] The minor quantities of by-products were attributed to secondary reactions involving the products of the three main reactions.[39]

Figure 1 displays the experimentally measured data points for CO_2 conversion alongside the yields of CH_3OH and CO compared to the equilibrium values.[49] The carbon balances for these primary products consistently exceeded 97% under the tested conditions. The measured data values can be found in Table S1. During the experiments, CO_2 conversion began at low values at 180°C, gradually approaching the equilibrium values at approximately 260°C and beyond. The yields of both CH_3OH and CO increased near equilibrium within the same temperature range. Consequently, the data collected between 180 and 260°C were suitable for the kinetics analysis for two reasons: (i) they were obtained at low CO_2 conversions, which is essential for fitting at a differential condition; and (ii) they were gathered at low yields of CH_3OH and CO, which reduces the potential of artifacts related to product saturation.[50]

3.2. Kinetics analysis

In this study, we considered two independent reactions: CO_2 methanol synthesis and RWGS. The apparent activation energies for these processes were calculated from the Arrhenius plots shown in Figure 2, focusing on the behavior of the reactions as they were approaching equilibrium at the lower temperatures. The reaction rates were measured in mol·s^{-1}/kg$_{cat}$, and the pressure was expressed in bar. The experimental data were adequately populated around the fitted lines, yielding a coefficient of determination (R^2) of 82% for Reaction 1 and 96% for Reaction 2. As detailed in Table 2, the apparent activation energies were determined to be 47.5 kJ·mol^{-1} for Reaction 1 and 106.2 kJ·mol^{-1} for Reaction 2. Both values were lower than those reported for recent Cu/ZnO/Al_2O_3 catalysts, typically around 65 and 110 kJ/mol.[51,52] The enhanced activity of the zeolite-supported Cu/ZnO catalyst compared to Cu/ZnO/Al_2O_3 was attributed to the smaller size of metal particles, and the electronic charge modification by ZnO. Previous *in situ* spectroscopic studies have indicated that the transformations of carbonyl and formate reaction intermediates occurred rapidly, while the accumulation of carbonate compounds and water was inhibited on this material.[23]

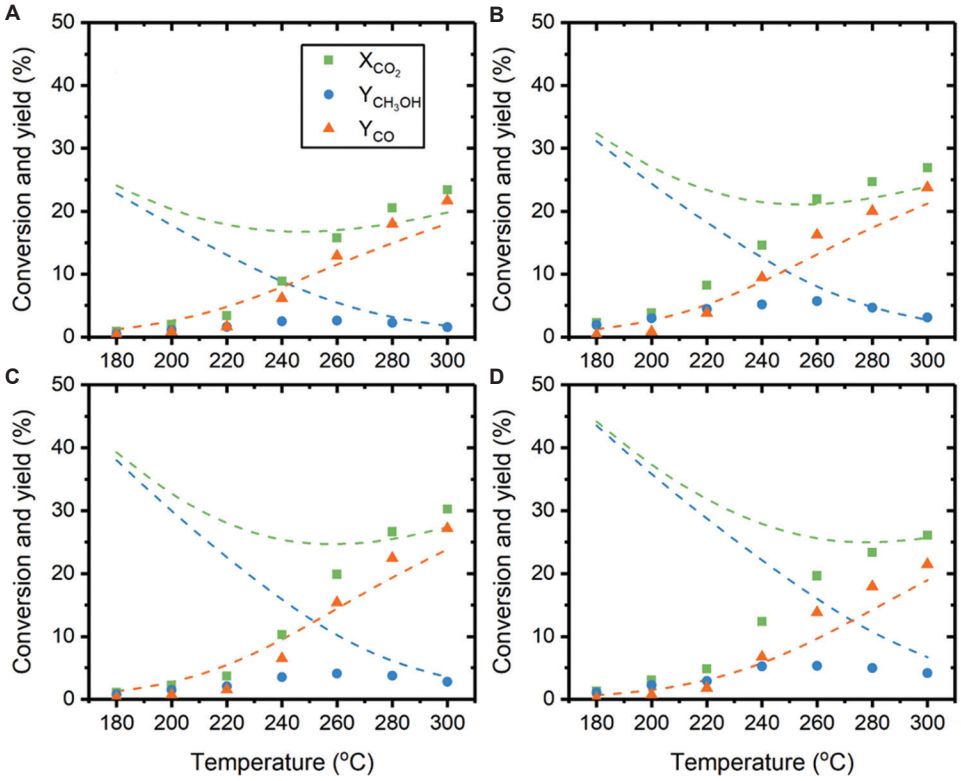

Figure 1. The conversion of carbon dioxide (CO_2), yields of methanol (CH_3OH), and carbon oxide (CO). Results at 3 MPa with feed CO_2/H_2 ratios of (A) 1:2, (B) 1:3, (C) 1:4, and at (D) 5 MPa with CO_2/H_2 ratio = 1:3. The scatterers represent experimental data; the dotted lines are calculated equilibrium values.

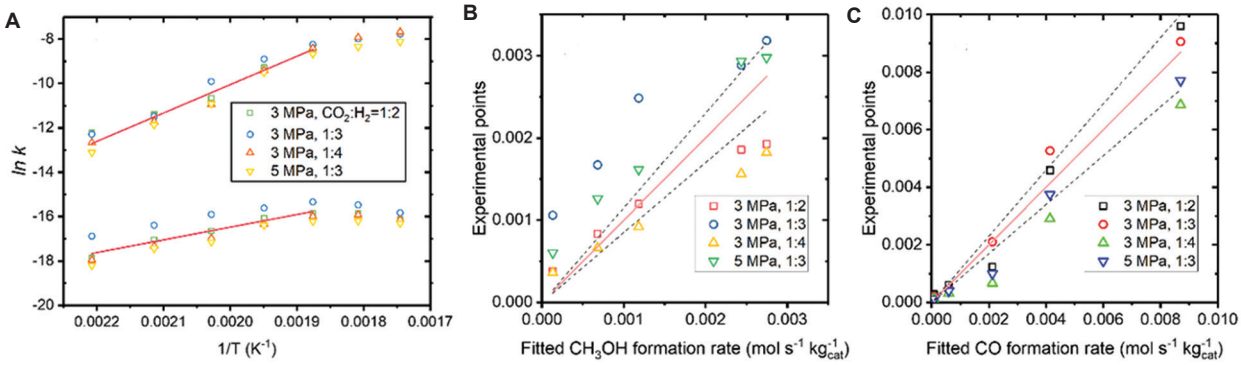

Figure 2. Kinetics fittings to the experimental data points. (A) Arrhenius plots. (B and C) Parity plots of the reaction rates by the Vanden Bussche and Froment model, with the dotted lines representing ±15% deviations.

Table 1. The catalytic reactions under study

Reaction	Equation	ΔH° (kJ·mol^{-1})	Equilibrium expressions	Reaction no.
Carbon dioxide to methanol synthesis	CO_2+3 H_2⇔CH_3OH+H_2O	−49.4	$\ln K_1$=7,313.8/T−24.574[a] $\log K_1$=3,176.3/T−10.672[b]	1
Reversed water–gas shift	CO_2+H_2⇔CO+H_2O	41.1	$\ln K_2$ = −4,670.2/T+4.4477[a] $\log K_2$ = −2,082.2/T+1.9316[b]	2
Syngas to methanol	CO+2 H_2⇔CH_3OH	−90.5	$\ln K_3$=6,011.9/T−19.706[a] $\log K_3$=2,610.9T−8.5583[b]	3

Notes: [a]Equilibrium constants K are calculated based on partial pressures in bar. [b]Represented in $\log_{10}$, for a direct comparison with the widely cited data by Graaf *et al.*[48] (Table S2).

Table 2. The apparent reaction activation energies from Arrhenius plots

Reaction name	Reaction equation	Arrhenius parameters[a]	E_a (kJ·mol^{-1})	Equation no.
Carbon dioxide to methanol synthesis	CO_2+3 H_2⇔CH_3OH+H_2O	$\ln k_1 = -5{,}715.4/T-6.3762$	47.5	1
Reversed water–gas shift	CO_2+H_2⇔CO+H_2O	$\ln k_2 = -12{,}775/T+14.1949$	106.2	2
Syngas to methanol	CO+2 H_2⇔CH_3OH	-	-	3

Note: [a]The reaction rates are represented in mol kg_{cat}^{-1}/s.

The Cu/ZnO/SPP-zeolite catalyst showed a higher activation energy for the RWGS reaction than the CO_2 to methanol reaction. As the reactions approached the equilibrium conditions, Reaction 1 was more significantly inhibited by Reaction 2, as evidenced by the deviations of experimental data from the fitted lines in Figure 2A at higher temperatures (280 and 300°C). These data points dropped.

The reaction mechanisms, including the reaction pathways, intermediates, and types of catalytic sites involved, as well as associated micro-kinetics, vary with different materials and reaction conditions. These aspects are currently under extensive investigation.[8,36,42,44,53,54] The formation of CO_2 to methanol and the simultaneous production of CO involve two primary pathways: The formate route and the RWGS route.[5,8,55-58] Distinct reaction intermediates formed and were consumed on the active sites with preferences and speeds that varied based on the catalyst used. A widely accepted reaction mechanism diagram is presented in Figure S1.[5] For zeolite-confined small Cu clusters, several adsorbed species were detected using *in situ* Fourier transform infrared spectroscopy (Bruker Vertex V70, US). These include HCOO* and HCOOH*, which are exclusive to the formate route, and CO* and HCO*, which are associated with the RWGS route. Both routes joined with H_3CO* before CH_3OH formed and desorbed. In the case of 1–2 nm Cu clusters, intermediates from the formate route were formed and consumed more quickly than those from the RWGS route, indicating that the formate route was preferential.[22] On the Cu/ZnO/SPP-zeolite catalyst, all the identified adsorbed species underwent rapid turnover, while the coverages of CO_2* and H_2O* remained consistently low.[23]

In accordance with the reaction mechanism, the micro-kinetics formulated by Grabow and Mavrikakis[59] involve 49 elementary reaction steps. In the reaction network, adsorbed CO* species can form through a redox-type cleavage of a C=O bond,[60] or via the dehydration of the hydrocarboxyl intermediate COOH*. These species either desorb as the CO product or react further with adsorbed H*. The VBF model[41] additionally assumes that CO_2 is the direct carbon source of CH_3OH, and all reactions, such as CO_2 hydrogenation to CH_3OH and CO, H_2 splitting, and water inhibition, occur at the same site. Recent assessments, supported by new experimental data and theoretical simulations, have confirmed the feasibility of the one-site model in the conditional range that covers the present tests.[36,42,51,54,61] For insights into multi-site models, one can refer to the refined fittings based on data collected for Cu/ZnO/Al_2O_3 catalysts.[51]

Table 3. Fitted parameters according to the Vanden Bussche and Froment model

Parameter	A	B
k_1	1.12E+06	47,500
k_2	1.62E+13	−106,200
K_3	3450	0
K_4	0.49	17,197
K_5	5.28E−07	112,000

The fitting of the VBF kinetics equations was also performed using data obtained at the low reaction temperatures (180–260°C). In the VBF model, the rates of the Reactions 1 and 2 are presented as follows in Equations V and VI:

$$r_1 = \frac{k_1 * P_{CO_2} * P_{H_2} * \left(1 - \frac{1}{K_{1eq.}} * \frac{P_{CH_3OH} * P_{H_2O}}{P_{CO_2} * P_{H_2}^{\ 3}}\right)}{\left(1 + K_3 * \left(P_{H_2O} / P_{H_2}\right) + K_4 * \sqrt{P_{H_2}} + K_5 * P_{H_2O}\right)^3} \quad \text{(V)}$$

$$r_2 = \frac{k_2 * P_{CO_2} * \left(1 - \frac{1}{K_{2eq.}} * \frac{P_{CO} * P_{H_2O}}{P_{CO_2} * P_{H_2}}\right)}{\left(1 + K_3 * \left(P_{H_2O} / P_{H_2}\right) + K_4 * \sqrt{P_{H_2}} + K_5 * P_{H_2O}\right)} \quad \text{(VI)}$$

In Equations V and VI, the parameters k_1 and k_2 represent the kinetic factors related to the turnover of the respective reactants and intermediates, while K_3, K_4, and K_5 denote the adsorption equilibria of H_2O, H_2, and their reaction intermediates. According to Arrhenius or Van't Hoff equations, these parameters exhibit temperature dependency in the form of k_i or $K_i = A_i * e^{Bi/RT}$.[41] By fitting the equations to the experimental data points, the parameters were determined and are listed in Table 3. The fitted curves compared to the experimental data points

are presented in Supporting Information Figure S2. The parity plots of fitted r_1 and r_2 are illustrated in Figure 2. These plots indicate that the fitted model reasonably represents the average values of the experimental points. However, there are somewhat larger deviations, particularly in the lower temperature range, due to measurement errors. Achieving better fits would require a significantly larger set of experimental measurements across various feed flows and different temperature and pressure conditions. For now, the derived average values can be utilized for reactor simulations. Fortunately, the fitting quality around 230°C is acceptable, which aligns with practical operational conditions. We initially optimized the reactor and process operations using these preliminary fittings, expecting sufficient data to be gathered for further refining the results. Alternatively, other types of models that incorporate more details of the reaction mechanisms, such as the two-site model by Graaf,[48] which is also widely applied in engineering designs, or more recent models that explore various reaction paths toward CH_3OH and CO, should also be considered for kinetic analyses.[59,60]

3.3. Single-path performance in a reactor tube

Single-path performances were evaluated using the provided VBF kinetic parameters at a pressure of 50 bar on various feed compositions. This was conducted in an adiabatic reactor tube with an inlet temperature of 230°C. The tube configuration and operational conditions are detailed in Table 4. It was assumed that the catalyst has a density of 1,200 kg·m^{-3} and is packed in a bed with a porosity of 0.4. These values are typical for zeolite-based catalysts.

Figure 3 presents the test results using various feed compositions. One of the feeds consisted of a 1:3 mixture of CO_2 and H_2, which served as the fresh feed. The other feeds contained increasing amounts of H_2, CO, and H_2O, with their compositions approaching those combined with recycled streams. The reactor tube was immersed in a cooling fluid maintained at 230°C, with a heat flux of 2,000 Watt·m^{-2}/°C, a realistic value for practice. Throughout these tests, the reaction heats did not pose any issue, with the highest temperature increase being approximately 1°C near the reactor inlet. Beyond that part, the temperature stabilized at 230°C for the latter half of the tube. The reaction flows achieved equilibrium compositions as they approached the outlet for the different tested feed compositions. As anticipated, using recycled CO and H_2 resulted in a higher yield of CH_3OH than using the pure CO_2/H_2 feed. The tests were consistently stable, which can be interpreted as validating the parameter fittings within the one-site VBF kinetic model. The resulting values for

Table 4. Configuration of the reactor tube and operational conditions

Parameters	Values
Reactor tube configuration	
Length (m)	8
Diameter (m)	0.0375
Bed porosity	0.4
Catalyst density (kg m^{-3})	1,200
Catalyst weight (kg)	6.4
Cooling fluid temperature (°C)	230
Heat flux (Watt m^{-2}/°C)	2,000
Feed	
Total flow (kmol h^{-1})	0.1263
Compositions (mol ratios)	
Composition 1 (CO_2/H_2)	1/3
Composition 2 (CO_2/H_2)	1/4
Composition 3 ($CO_2/CO/H_2$)	0.9/0.1/4
Composition 4 ($CO_2/CO/H_2/H_2O$)	0.9/0.05/4/0.0.05
Pressure (bar)	50
Temperature (°C)	230
Results	
Composition 1	
X_{CO2} (%)	31.4
S_{CH3OH} (%)	87.9
STY_{CH3OH} (kg kg_{cat}^{-1}/h)	1.75
Composition 2	
X_{CO2} (%)	38.1
S_{CH3OH} (%)	89.8
STY_{CH3OH} (kg kg_{cat}^{-1}/h)	2.16
Composition 3	
X_{CO2} (%)	42.4
S_{CH3OH} (%)	89.9
STY_{CH3OH} (kg kg_{cat}^{-1}/h)	2.41
Composition 4	
X_{CO2} (%)	39.7
S_{CH3OH} (%)	90.1
STY_{CH3OH} (kg kg_{cat}^{-1}/h)	2.26

Abbreviation: STY: Space-time yield.

CO_2 conversion and CH_3OH yields are also summarized in Table 4. With the fresh feed, the space-time yield of CH_3OH reached 1.75 kg·kg_{cat}^{-1}/h. This yield is notably higher than that reported for recent $Cu/ZnO/Al_2O_3$ catalysts. In the benchmark tests involving a typical commercial $Cu/ZnO/Al_2O_3$ catalyst under comparable conditions of 250°C and 50 bar, the reported space-time yield was 1.14 kg·kg_{cat}^{-1}/h (Tables S3 and 4 for a direct comparison).[62]

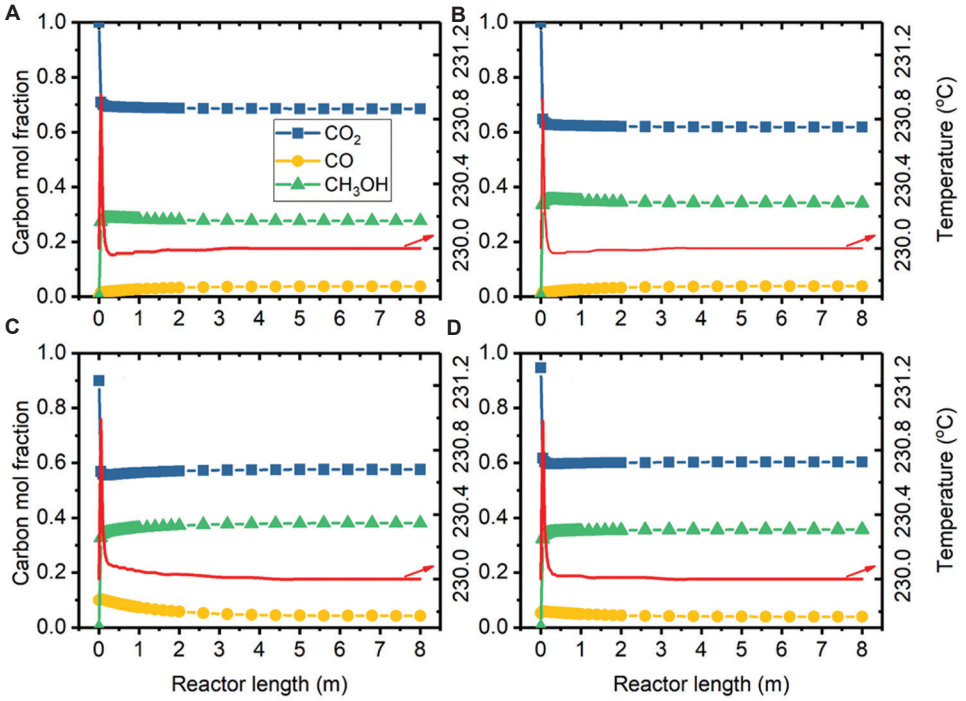

Figure 3. Temperature profile and molar fraction profile of the reaction flows in a single path of different feed compositions in the reactor tube at 50 bar. (A) CO_2/H_2 = 1:3, (B) CO_2/H_2 = 1:4; (C) $CO_2/CO/H_2$ = 0.9:0.1:4, and (D) $CO_2/CO/H_2/H_2O$ = 0.9:0.05:4:0.05.

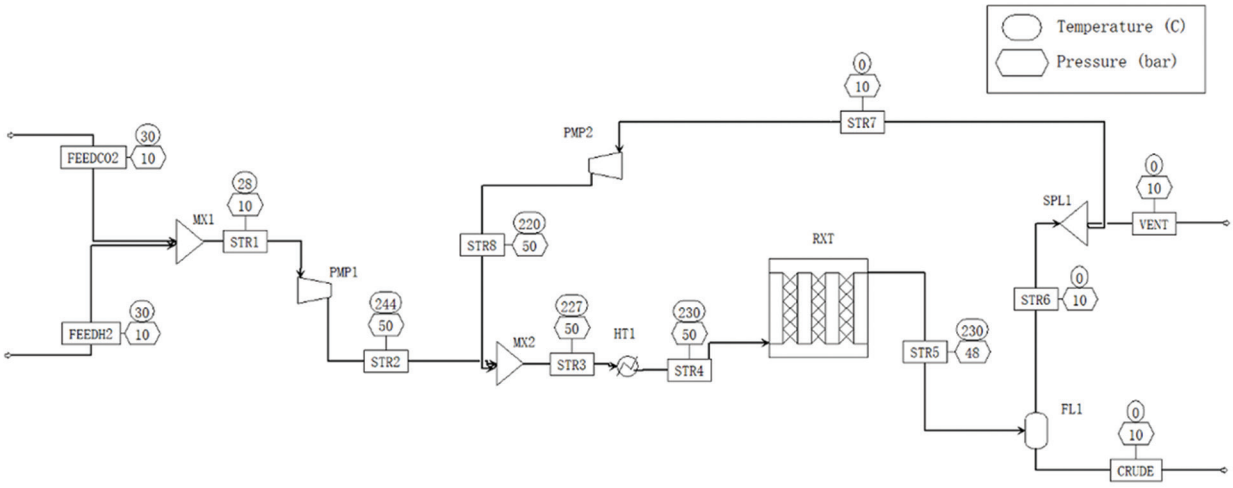

Figure 4. Flowsheet of the process with a single vapor recycling loop for the optimization of methanol yield

3.4. Process with one recycling loop

A process equipped with a single recycling loop was constructed, as shown in Figure 4. Assumptions regarding the configurations included the following:

(i) The reactor consisted of 200 tubes, each 8 m long and 0.0375 m in diameter. The tubes were immersed in a coolant flow maintained at 230°C with a heat flux of 2,000 Watt·m^{-2}/°C. The preparation and energy cost of the cooling fluid have been excluded from consideration. The pressure reduction across the reactor was artificially set to 2 bar.

(ii) The feed flow was composed of a 1:3 mixture of CO_2/H_2 at a flow rate of 25.2 kmol/h, corresponding to a CO_2 utilization scale of 2,000 NT/an.

(iii) The vapor/liquid separation of the product flow was simulated using a flash evaporator, which achieved equilibrium at 0°C and 10 bar. This treatment ensured

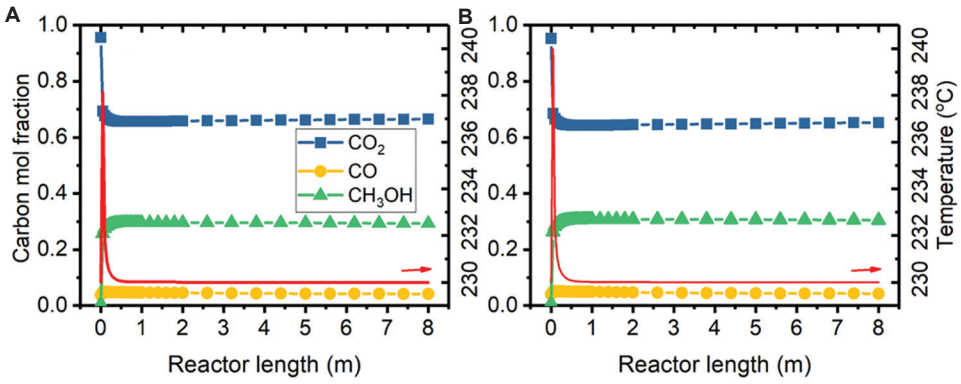

Figure 5. Temperature profile and the molar fraction profile of the reaction flow in the reactor. (A) 0.90 and (B) 0.95 ratios of product vapor recycling.

Table 5. The conditions and results of the process simulation with a single recycling loop at 0.90 and 0.95 recycling ratios

Parameters	Values	
Reactor configuration		
Tube number	200	
Length (m)	8	
Diameter (m)	0.0375	
Bed porosity	0.4	
Catalyst density (kg m^{-3})	1,200	
Catalyst weight (kg)	1,272	
Cooling fluid temperature (°C)	230	
Heat flux (Watt m^{-2}/°C)	2,000	
Feed		
Total flow (kmol/h)	25.2	
Compositions (mol ratios): CO_2/H_2	1/3	
Results	0.90 vapor recycling	0.95 recycling
Process		
X_{CO2} (%)	80.2	88.7
Y_{CH3OH} (%)	78.9	88.0
Reactor		
X_{CO2} (%)	30.4	31.5
Y_{CH3OH} (%)	28.7	29.8
STY_{CH3OH} (kg kg_{cat}^{-1}/h)	1.25	1.39

Abbreviation: STY: Space-time yield.

that <1% of CH_3OH and H_2O were recycled to the reactor, while the CO_2 concentration in the crude liquid was controllable at a similar level. These values were considered realistic in practice. The energy cost associated with the separation has not been analyzed at this stage. It is assumed that heavier by-products, such as ethanol, formaldehyde, etc., will remain in the crude liquid stream for further refinement.

Table 6. The mass flow of the vent and crude liquid in comparison with the feed

Mass flow	Feed	90% vapor recycling		95% vapor recycling	
		Vent	Crude	Vent	Crude
CO_2	277.3	50.4	4.4	26.5	4.7
H_2	38.1	7.8	-	4.4	-
CH_3OH	-	0.4	159.2	0.2	177.7
CO	-	2.0	-	1.1	-
H_2O	-	0.0	91.0	0.0	100.7
Total	315.4	60.7	254.6	32.3	283.1
		315.4		315.4	

Note: All values represented as kg/h, unless stated otherwise.

(iv) Two recycling ratios of the vapor stream were examined: 0.90 and 0.95. Light by-products like methane were vented to prevent their accumulation in the reaction stream.

Overall, the energy costs associated with the feed mixing and pressurization, product separation and refining, and other unit operations have not been analyzed. Therefore, the purpose of this process design is solely to evaluate and optimize the conversion of CO_2 and the yield of CH_3OH, rather than to assess energy costs. Table 5 summarizes the operational conditions and the simulation results.

The CO_2 conversion with 90% recycling of the vapor product could surpass 80%, with CH_3OH yields also approaching 80%. The reactor's single path achieved approximately 30% CO_2 conversion, resulting in CH_3OH production with a space-time yield at 1.25–1.39 $kg \cdot kg_{cat}^{-1}/h$. The temperature increased by about 10°C at the reactor inlet zone and stabilized in the second half of the reactor, as shown in Figure 5. The lost carbon was found in the vent and the crude product. Table 6 presents the mass flows of the feeds and outputs. The test conducted with 95%

recycling yielded better results in terms of CO_2 conversion and CH_3OH yield, making it a feasible option, provided that the energy costs analysis supports the operation. In both conditions, the crude liquid products contained approximately 62.5 wt% methanol in water, and 1.6–1.7 wt% CO_2.

4. Conclusion

The Cu/ZnO/SPP-zeolite catalyst, featuring smaller Cu particles encapsulated within the mesopores of the pure-silica SPP zeolite and modified with ZnO species, demonstrated faster kinetics and lower activation energies in the hydrogenation of CO_2 to CH_3OH and CO compared to the conventional $Cu/ZnO/Al_2O_3$ catalysts. This observation aligns with previous *in situ* spectroscopic studies conducted by our group on the same material and broader research on the effects of reduced metal sizes and enhanced surface charges.

The one-site kinetics model developed by VBF was utilized to fit the experimental reaction rates obtained from a fixed-bed microreactor. Acceptable kinetics parameters and parameters regarding H_2O and H_2 adsorption were determined and used to simulate the once-through and recycled reaction flows in a tubular reactor. By leveraging the high activity of the new catalyst, a space-time yield of 1.75 $kg{\cdot}kg_{cat}^{-1}/h$ methanol was achieved in a single tube simulation with fresh feed composed of CO_2 and $3H_2$ at 230°C and 50 bar. In the optimized process with a recycling loop, over 80% CO_2 conversion with nearly 80% CH_3OH yield was achieved with a 90% recycling of the vapor product at a space-time yield of 1.25 $kg{\cdot}kg_{cat}^{-1}/h$ in the process segment, surpassing the performance of the $Cu/ZnO/Al_2O_3$ catalyst. At a scale of 2,000 NT/annum CO_2 feed, it was possible to produce 1,836 NT/annum crude containing 62.5 wt% methanol. A 95% recycling rate was also conducted, resulting in slight improvements in both CO_2 conversion and CH_3OH yield.

However, the refinement of the crude product and the energy consumption associated with the process has not yet been analyzed in the present work. The choice of unit operations significantly impacts the results and will be a focus of future process optimization efforts.

The fitting of the kinetics parameters still exhibited substantial deviations from the available experimental data points. More precisely, the available data points lack sufficient accuracy. As more experimental measurements become available, the parameters can be refined.

Numerous Cu-based and non-Cu-based catalysts, aside from $Cu/ZnO/Al_2O_3$, have been intensively studied for their optimal performances for CO_2 hydrogenation to methanol and other upgraded hydrocarbon products.[63] However, few studies have progressed in investigating reaction kinetics and process optimization. The present analysis serves as a valuable supplement to the existing research, with the anticipation that the dataset will expand to encompass a broader range of catalysts and parameters with refined accuracy.

Acknowledgments

None.

Funding

This work was funded by the Natural Science Foundation of Shandong Province, China (ZR2022MB053 and ZR2022QB216).

Conflict of interest

The authors declare that they have no competing interests.

Author contributions

Conceptualization: Qiaolin Lang, Xiaobo Yang, Guangying Fu

Investigation: All authors

Methodology: Qiaolin Lang, Xiaobo Yang, Guangying Fu

Writing–original draft: Qiaolin Lang, Xiaobo Yang, Guangying Fu

Writing–review & editing: Qiaolin Lang, Xiaobo Yang, Guangying Fu

Ethics approval and consent to participate

Not applicable.

Consent for publication

Not applicable.

Availability of data

Additional experimental data and results of the kinetics analysis are provided in the Supplementary File.

References

1. Ueckerdt F, Bauer C, Dirnaichner A, Everall J, Sacchi R, Luderer G. Potential and risks of hydrogen-based e-fuels in climate change mitigation. *Nat Clim Change.* 2021;11(5):384-393.

   doi: 10.1038/s41558-021-01032-7

2. Shih CF, Zhang T, Li J, Bai C. Powering the future with liquid sunshine. *Joule.* 2018;2(10):1925-1949.

   doi: 10.1016/j.joule.2018.08.016

3. Ahmad T, Liu S, Sajid M, *et al.* Electrochemical CO_2

reduction to C_2+ products using Cu-based electrocatalysts: A review. *Nano Res Energy.* 2022;1:9120021.

doi: 10.26599/NRE.2022.9120021

4. Li K, Xu J, Zheng T, *et al*. *In situ* dynamic construction of a copper tin sulfide catalyst for high-performance electrochemical CO_2 conversion to formate. *ACS Catal.* 2022;12(16):9922-9932.

doi: 10.1021/acscatal.2c02627

5. Zhong J, Yang X, Wu Z, Liang B, Huang Y, Zhang T. State of the art and perspectives in heterogeneous catalysis of CO_2 hydrogenation to methanol. *Chem Soc Rev.* 2020;49(5):1385-1413.

doi: 10.1039/C9CS00614A

6. Hong F, Qi Y, Yang Z, *et al*. Recent advances of CO_2 hydrogenation to methanol. *DeCarbon.* 2025;8:100111.

doi: 10.1016/j.decarb.2025.100111

7. George Olah CO_2 to Renewable Methanol Plant, Reykjanes, Iceland. Available from: https://www.carbonrecycling.is [Last accessed on 2025 Sep 09].

8. Behrens M, Studt F, Kasatkin I, *et al*. The active site of methanol synthesis over Cu/ZnO/Al_2O_3 industrial catalysts. *Science.* 2012;336(6083):893-897.

doi: 10.1126/science.1219831

9. Lin TC, Nolen MA, Farberow CA, Kwon S, Bhan A. Mechanistic and kinetic relevance of hydrogen and water in CO_2 hydrogenation on Cu-based catalysts. *J Catal.* 2025;443:115936.

doi: 10.1016/j.jcat.2024.115936

10. Wang M, Zhang G, Wang H, *al*. Understanding and tuning the effects of H_2O on catalytic CO and CO_2 hydrogenation. *Chem Rev.* 2024;124(21):12006-12085.

doi: 10.1021/acs.chemrev.4c00282

11. Toyir J, Miloua R, Elkadri NE, *et al*. Sustainable process for the production of methanol from CO_2 and H_2 using Cu/ZnO-based multicomponent catalyst. *Phys Procedia.* 2009;2(3):1075-1079.

doi: 10.1016/j.phpro.2009.11.065

12. Zhang S, Wu Z, Liu X, *et al*. A short review of recent advances in direct CO_2 hydrogenation to alcohols. *Topics Catal.* 2021;*64*(5):371-394.

doi: 10.1007/s11244-020-01405-w

13. Gao P, Zhang L, Li S, Zhou Z, Sun Y. Novel heterogeneous catalysts for CO_2 hydrogenation to liquid fuels. *ACS Cent Sci.* 2020;6(10):1657-1670.

doi: 10.1021/acscentsci.0c00976

14. Gao P, Li S, Bu X, *et al*. Direct conversion of CO_2 into liquid fuels with high selectivity over a bifunctional catalyst. *Nat Chem.* 2017;9(10):1019-1024.

doi: 10.1038/nchem.2794

15. Wang J, Wang T, Xi Y, Gao G, Sun P, Li F. *In-situ*-formed potassium-modified nickel-zinc carbide boosts production of higher alcohols beyond CH_4 in CO_2 hydrogenation. *Angew Chem Int Ed Engl.* 2023;62(42):e202311335.

doi: 10.1002/anie.202311335

16. Chen J, Ma J, Huang T, *et al*. Iridium-free high-entropy alloy for acidic water oxidation at high current densities. *Angew Chem Int Ed Engl.* 2025;64(21):e202503330.

doi: 10.1002/anie.202503330

17. Su D, Wang Y, Sheng H, *et al*. Efficient amine-assisted CO_2 hydrogenation to methanol co-catalyzed by metallic and oxidized sites within ruthenium clusters. *Nat Commun.* 2025;16(1):590.

doi: 10.1038/s41467-025-55837-7

18. Wang Y, Wang C, Wang L, Wang L, Xiao FS. Zeolite fixed metal nanoparticles: New perspective in catalysis. *Acc Chem Res.* 2021;54(11):2579-2590.

doi: 10.1021/acs.accounts.1c00074

19. Liu L, Corma A. Metal catalysts for heterogeneous catalysis: From single atoms to nanoclusters and nanoparticles. *Chem Rev.* 2018;118(10):4981-5079.

doi: 10.1021/acs.chemrev.7b00776

20. Xia Y, Yang X. Toward cost-effective and sustainable use of precious metals in heterogeneous catalysts. *Acc Chem Res.* 2017;50(3):450-454.

doi: 10.1021/acs.accounts.6b00469

21. Kosinov N, Liu C, Hensen EJM, Pidko EA. Engineering of transition metal catalysts confined in zeolites. *Chem Mater.* 2018;30(10):3177-3198.

doi: 10.1021/acs.chemmater.8b01311

22. Ding R, Fu G, Wang S, *et al*. The activity of ultrafine cu clusters encapsulated in nano-zeolite for selective hydrogenation of CO_2 to methanol. *Catalysts.* 2022;12(11):1296.

doi: 10.3390/catal12111296

23. Liu X, Fu G, Lang Q, *et al*. Reaction intermediates recognized by *in situ* FTIR spectroscopy in CO_2 hydrogenation over the Cu/ZnO/SPP-zeolite catalyst. *RSC Appl Interfaces.* 2025;2(1):114-121.

doi: 10.1039/d4lf00266k

24. Zhang X, Liu JX, Zijlstra B, *et al*. Optimum Cu nanoparticle catalysts for CO_2 hydrogenation towards methanol. *Nano Energy.* 2018;43:200-209.

doi: 10.1016/j.nanoen.2017.11.021

25. Gautam S, Dharamvir K, Goel N. CO_2 adsorption and activation over medium sized Cu_n (n=7, 13 and 19) clusters: A density functional study. *Comput Theor Chem.* 2013;1009:8-16.

doi: 10.1016/j.comptc.2012.12.010

26. Yang B, Liu C, Halder A, *et al*. Copper cluster size effect in methanol synthesis from CO_2. *J Phys Chem C.* 2017;121(19):10406-10412.

doi: 10.1021/acs.jpcc.7b01835

27. Liu C, Yang B, Tyo E, *et al*. Carbon dioxide conversion to methanol over size-selected Cu_4 clusters at low pressures. *J Amer Chem Soc.* 2015;137(27):8676-8679.

doi: 10.1021/jacs.5b03668

28. Li G, Vassilev P, Sanchez-Sanchez M, Lercher JA, Hensen EJM, Pidko EA. Stability and reactivity of copper oxo-clusters in ZSM-5 zeolite for selective methane oxidation to methanol. *J Catal.* 2016;338:305-312.

doi: 10.1016/j.jcat.2016.03.014

29. Cui WG, Li YT, Yu L, Zhang H, Hu TL. Zeolite-encapsulated ultrasmall Cu/ZnO_x nanoparticles for the hydrogenation of CO_2 to methanol. *ACS Appl Mater Interfaces.* 2021;13(16):18693-18703.

doi: 10.1021/acsami.1c00432

30. Ding L, Shi T, Gu J, *et al*. CO_2 hydrogenation to ethanol over Cu@Na-Beta. *Chem.* 2020;6(10):2673-2689.

doi: 10.1016/j.chempr.2020.07.001

31. Mehla S, Kandjani AE, Babarao R, *et al*. Porous crystalline frameworks for thermocatalytic CO_2 reduction: An emerging paradigm. *Energy Environ Sci.* 2021;14(1):320-352.

doi: 10.1039/D0EE01882A

32. Stangeland K, Li H, Yu Z. Thermodynamic analysis of chemical and phase equilibria in CO_2 hydrogenation to methanol, dimethyl ether, and higher alcohols. *Ind Eng Chem Res.* 2018;57(11):4081-4094.

doi: 10.1021/acs.iecr.7b04866

33. Jia C, Gao J, Dai Y, Zhang J, Yang Y. The thermodynamics analysis and experimental validation for complicated systems in CO_2 hydrogenation process. *J Energy Chem.* 2016;25(6):1027-1037.

doi: 10.1016/j.jechem.2016.10.003

34. Mbatha S, Thomas S, Parkhomenko K, *et al*. Development of an improved kinetic model for CO_2 hydrogenation to methanol. *Catalysts.* 2023;13(10):1349.

doi: 10.3390/catal13101349

35. Poto S, Vico van Berkel D, Gallucci F, Fernanda Neira d'Angelo, M. Kinetic modelling of the methanol synthesis from CO_2 and H_2 over a CuO/CeO_2/ZrO_2 catalyst: The role of CO_2 and CO hydrogenation. *Chem Eng J.* 2022;435:134946.

doi: 10.1016/j.cej.2022.134946

36. Nestler F, Schütze AR, Ouda M, *et al*. Kinetic modelling of methanol synthesis over commercial catalysts: A critical assessment. *Chem Eng J.* 2020;394:124881.

doi: 10.1016/j.cej.2020.124881

37. Seidel C, Jörke A, Vollbrecht B, Seidel-Morgenstern A, Kienle A. Kinetic modeling of methanol synthesis from renewable resources. *Chem Eng Sci.* 2018;175:130-138.

doi: 10.1016/j.ces.2017.09.043

38. Portha JF, Parkhomenko K, Kobl K, *et al*. Kinetics of methanol synthesis from carbon dioxide hydrogenation over copper-zinc oxide catalysts. *Ind Eng Chem Res.* 2017;56(45):13133-13145.

doi: 10.1021/acs.iecr.7b01323

39. Park N, Park MJ, Lee YJ, Ha KS, Jun KW. Kinetic modeling of methanol synthesis over commercial catalysts based on three-site adsorption. *Fuel Process Tech.* 2014;125:139-147.

doi: 10.1016/j.fuproc.2014.03.041

40. Kubota T, Hayakawa I, Mabuse H, *et al*. Kinetic study of methanol synthesis from carbon dioxide and hydrogen. *Appl Organometal Chem.* 2001;15(2):121-126.

doi: 10.1002/1099-0739(200102)15:2<121::AID-AOC106>3.0.CO;2-3

41. Bussche KMV, Froment GF. A steady-state kinetic model for methanol synthesis and the water gas shift reaction on a commercial Cu/ZnO/Al_2O_3 catalyst. *J Catal.* 1996;161(1):1-10.

doi: 10.1006/jcat.1996.0156

42. Slotboom Y, Bos MJ, Pieper J, *et al*. Critical assessment of steady-state kinetic models for the synthesis of methanol over an industrial Cu/ZnO/Al_2O_3 catalyst. *Chem Eng J.* 2020;389:124181.

doi: 10.1016/j.cej.2020.124181

43. Leonzio G, Zondervan E, Foscolo PU. Methanol production by CO_2 hydrogenation: Analysis and simulation of reactor performance. *Int J Hydrogen Energy.* 2019;44(16):7915-7933.

doi: 10.1016/j.ijhydene.2019.02.056

44. Kyrimis S, Potter ME, Raja R, Armstrong LM. Understanding catalytic CO_2 and CO conversion into methanol using computational fluid dynamics. *Faraday Discus.* 2021;230:100-123.

doi: 10.1039/D0FD00136H

45. Ghosh, S, Sebastian, J, Olsson, L, Creaser, D. Experimental and kinetic modeling studies of methanol synthesis from CO_2 hydrogenation using In_2O_3 catalyst. *Chem Eng J.* 2021;416:129120.

doi: 10.1016/j.cej.2021.129120

46. Ahmad K, Upadhyayula S. Kinetics of CO_2 hydrogenation to methanol over silica supported intermetallic Ga_3Ni_5 catalyst in a continuous differential fixed bed reactor. *Internat J Hydrogen Energy.* 2020;45(1):1140-1150.

doi: 10.1016/j.ijhydene.2019.10.156

47. Zhang X, Liu D, Xu D, *et al*. Synthesis of self-pillared zeolite nanosheets by repetitive branching. *Science.* 2012;336(6089):1684-1687.

doi: 10.1126/science.1221111

48. Graaf GH, Stamhuis EJ, Beenackers AAC. Kinetics of low-pressure methanol synthesis. *Chem Eng Sci.* 1988;43(12):3185-3195.

doi: 10.1016/0009-2509(88)85127-3

49. Hansen JB, Højlund Nielsen PE. Methanol synthesis. In: Ertl G, Knözinger H, Schüth F, Weitkamp J, editos. *Handbook of Heterogeneous Catalysis*. United States: Wiley; 2008. p. 2920-2949.

doi: 10.1002/9783527610044.hetcat0148

50. Sahibzada M, Metcalfe IS, Chadwick D. Methanol synthesis from $CO/CO_2/H_2$ over $Cu/ZnO/Al_2O_3$ at differential and finite conversions. *J Catal.* 1998;174(2):111-118.

doi: 10.1006/jcat.1998.1964

51. Bisotti F, Fedeli M, Prifti K, *et al*. Century of technology trends in methanol synthesis: Any need for kinetics refitting? *Ind Eng Chem Res.* 2021;60(44):16032-16053.

doi: 10.1021/acs.iecr.1c02877

52. Ahmad K, Dabbawala AA, Polychronopoulou K, Anjum D, Gacesa M, Abi Jaoude M. Kinetic insights into methanol synthesis from CO_2 hydrogenation at atmospheric pressure over intermetallic Pd_2Ga catalyst. *Glob Chall.* 2024;8(10):2400159.

doi: 10.1002/gch2.202400159

53. Lacerda de Oliveira Campos B, Herrera Delgado K, Pitter S, Sauer J. Development of consistent kinetic models derived from a microkinetic model of the methanol synthesis. *Ind Eng Chem Res.* 2021;60(42):15074-15086.

doi: 10.1021/acs.iecr.1c02952

54. Lacerda de Oliveira Campos B, Herrera Delgado K, Wild S, Studt F, Pitter S, Sauer J. Surface reaction kinetics of the methanol synthesis and the water gas shift reaction on $Cu/ZnO/Al_2O_3$. *React Chem Eng.* 2021;6(5):868-887.

doi: 10.1039/D1RE00040C

55. Li HX, Yang LQQ, Chi ZY, *et al*. CO_2 Hydrogenation to methanol over $Cu/ZnO/Al_2O_3$ catalyst: Kinetic modeling based on either single- or dual-active site mechanism. *Catal Lett.* 2022;152(10):3110-3124.

doi: 10.1007/s10562-021-03913-0

56. Prašnikar A, Pavlišič A, Ruiz-Zepeda F, Kovač J, Likozar B. Mechanisms of copper-based catalyst deactivation during CO_2 reduction to methanol. *Ind Eng Chem Res.* 2019;58(29):13021-13029.

doi: 10.1021/acs.iecr.9b01898

57. Karelovic A, Galdames G, Medina JC, Yévenes C, Barra Y, Jiménez R. Mechanism and structure sensitivity of methanol synthesis from CO_2 over SiO_2-supported Cu nanoparticles. *J Catal.* 2019;369:415-426.

doi: 10.1016/j.jcat.2018.11.012

58. Lunkenbein T, Girgsdies F, Kandemir T, *et al*. Bridging the time gap: A Copper/Zinc Oxide/Aluminum Oxide catalyst for methanol synthesis studied under industrially relevant conditions and time scales. *Angew Chem Int Ed Engl.* 2016;55(41):12708-12712.

doi: 10.1002/anie.201603368

59. Grabow LC, Mavrikakis M. Mechanism of methanol synthesis on Cu through CO_2 and CO hydrogenation. *ACS Catal.* 2011;1(4):365-384.

doi: 10.1021/cs200055d

60. Ahmadi Khoshooei M, Wang X, Vitale G, *et al*. An active, stable cubic molybdenum carbide catalyst for the high-temperature reverse water-gas shift reaction. *Science.* 2024;384(6695):540-546.

doi: 10.1126/science.adl1260

61. Díez-Ramírez J, Díaz JA, Dorado F, Sánchez P. Kinetics of the hydrogenation of CO_2 to methanol at atmospheric pressure using a Pd-Cu-Zn/SiC catalyst. *Fuel Process Technol.* 2018;173:173-181.

doi: 10.1016/j.fuproc.2018.01.024

62. Ruland H, Song H, Laudenschleger D, *et al*. CO_2 hydrogenation with $Cu/ZnO/Al_2O_3$: A benchmark study. *ChemCatChem.* 2020;12(12):3216-3222.

doi: 10.1002/cctc.202000195

63. Ye J, Dimitratos N, Rossi LM, Thonemann N, Beale AM, Wojcieszak R. Hydrogenation of CO_2 for sustainable fuel and chemical production. *Science.* 2025;387(6737):eadn9388.

doi: 10.1126/science.adn9388